

## NUMERICAL STUDY ON THE SOLID-LIQUID RESIDENCE TIME DISTRIBUTION IN A COUNTER-CURRENT SCREW EXTRACTOR

Annemarie LEHR<sup>1</sup>, Gábor JANIGA<sup>2</sup>, Andreas SEIDEL-MORGENSTERN<sup>3</sup>,  
Dominique THÉVENIN<sup>4</sup>

<sup>1</sup> Department of Fluid Mechanics and Technical Flows, Faculty of Process and Systems Engineering, Otto von Guericke University Magdeburg, Universitätsplatz 2, 39106 Magdeburg, Tel.: +493916758109, E-mail: annemarie.lehr@ovgu.de

<sup>2</sup> Department of Fluid Mechanics and Technical Flows, Faculty of Process and Systems Engineering, Otto von Guericke University Magdeburg, E-mail: janiga@ovgu.de

<sup>3</sup> Max Planck Institute for Dynamics of Complex Technical Systems, E-mail: seidel-morgenstern@mpi-magdeburg.mpg.de

<sup>4</sup> Department of Fluid Mechanics and Technical Flows, Faculty of Process and Systems Engineering, Otto von Guericke University Magdeburg, E-mail: thevenin@ovgu.de

### ABSTRACT

The efficiency of extraction processes highly depends on the contact times and areas between the solvent and the valuable substance. In this study a solid-liquid screw extraction process of artemisinin from *Artemisia Annu* leaves has been investigated in a continuously working counter-current screw extractor with computational fluid dynamics (CFD). Artemisinin is increasingly used as efficient anti-malaria drug. Experimental data have been used for validation.

Mass transfer processes have been first neglected to decrease the complexity of the three-phase flow simulation. The soaked leaves have been represented by a rotating geometry with constant volume equal to the experimentally observed volume of the leaves. This enabled a simplified model by solving only a two-phase flow of liquid solvent and air. A Eulerian-based Volume of Fluid (VoF) model has been implemented to capture the free surface.

After four screw rotations a quasi-steady counter-current flow has been reached. Contact times have been observed by measuring the solvent residence time distribution (RTD) using the species transport method. A very good agreement between CFD and experiments could be found. Consequently, the contact area between leaves and solvent can be determined accurately by CFD, providing important information regarding the mass transfer behaviour during the extraction process.

**Keywords: computational fluid dynamics (CFD), extraction, residence time distribution**

### NOMENCLATURE

$D_o$	[m]	outer screw diameter
$D_i$	[m]	inner screw diameter
$L$	[m]	length
$N$	[-]	theoretical number of steps
$V$	[m <sup>3</sup> ]	volume
$\dot{m}$	[kg/s]	mass flow
$n$	[rpm]	screw rotation rate
$s$	[-]	storage factor
$t$	[min]	time
$w$	[m]	width
$\pi$	[-]	pi
$\rho$	[kg/m <sup>3</sup> ]	density
$\sigma$	[min]	standard deviation
$\sigma^2$	[min <sup>2</sup> ]	variance
$\tau$	[min]	residence time

### Subscripts and Superscripts

API	active pharmaceutical ingredients
CFD	computational fluid dynamics
CFL	convective courant number
CM	compartment model
E, R	extract, raffinate
EC	extraction cake
Exp	experimental
L, S	leaves, solvent
PD	perforated disc
SL	soaked leaves
RTD	residence time distribution
VoF	Volume of Fluid
$t$	total
$x, y, z$	axial (along the extractor), transversal, spanwise (coordinate)
–	temporal mean

## 1. INTRODUCTION

Gaining natural products by implementing solid-liquid extraction is used since centuries to obtain ingredients for perfumes or pharmaceutically active oils and waxes. Extracts of plant material contain lead compounds for nutraceutical or pharmaceutical applications. Nevertheless, the content of active ingredient in the feed material (e.g., leaves, flowers, branches) is usually only between 0.3 – 3 % [1]. This leads to an increasing interest in optimising the extraction efficiency of active ingredients.

In this work a continuous counter-current extraction process in a horizontal screw extractor has been implemented to obtain the active pharmaceutical ingredient (API) artemisinin from *Artemisia Annuua* leaves. Derivatives of artemisinin (e.g., artesunate) are well known as standard treatment against malaria, which is still the most deadly infectious disease worldwide [2,3].

The continuous counter-current process implemented here provides advantages compared to the generally used batch extraction. Fresh solvent and feed material are continuously fed into the device without dead times while loading or unloading the apparatus. The counter-current flow enables high contacting times and surfaces leading to higher extraction yields compared to batch processes.

The modular screw design allows high flexibility but leads also to challenges, in particular regarding the optimal screw configuration for specific process requirements [4]. In order to reduce experimental efforts Computational Fluid Dynamics (CFD) can be used for a fast optimisation since screw geometry and rotating speed, diameter and length of the extruder can be adapted easily in CFD. Nevertheless, the numerical complexity of the described extraction process with a gas, a liquid and a solid phase is very high. A transient 3D model is required [5].

The performance of continuous counter-current solid-liquid extraction processes is rarely published [6]. A representation with CFD simulations could not be found by the authors. More generally, solid-liquid extraction processes have been represented by transient 3D CFD models e.g., for the investigation of hydrodynamics of a tea bag during tea infusion [7]. Turgut et al. (2020) [8] presents a solid-liquid extraction of trans-resveratrol from grape cane powder in a semi-continuous pressurized water column under steady-state conditions regarding heat and momentum transfer. A three-phase flow extraction is reported by He and Zhang (2012) [9] who used a cyclone with turbulent air flow to perform liquid extraction from solid particles. A more similar configuration to the recent work is published by Shokrian et al. (2019) [10] who described a three phase flow in a horizontal rotating drum with a screw conveyor used for olive oil extraction. They represented the olive seeds as

particulate solids. A 3D CFD model is represented by Wang et al. [11] to represent a two-phase solid-liquid extraction of wax-containing brown coal in randomly packed beds and observe the particle size distribution. Further the CFD simulation of continuous two-phase protein extraction in a fluidized bed ion exchange system is reported by Dadashi et al. (2014) [12]. Several publications in the field of fluidized beds represent three-phase solid-liquid-gas flows in counter-current operation mode [13,14]. The usage of full 3D models for counter-current flows have been reported mainly for two-phase flows [15–17].

This work will introduce a model for representing a three-phase screw extraction process in counter-current mode by using a transient 3D model. To simplify this first model, mass transport processes between the phases have been neglected. For a later optimisation the contact times between liquid and solid phase are essential. They will be determined by quantifying their residence time distribution in the extractor. The species model is used in CFD since it solves only one additional transport equation, enabling short computational times. The aim is to improve our understanding of the process, ultimately increasing extraction efficiency of artemisinin.

## 2. MATHEMATICAL MODEL

The mean residence time and variance can be determined from the residence time distribution (RTD), which is a function of the length of the observed extruder. For measuring the RTD in a device, the stimulus response technique with pulse or stepwise input of a tracer is typically used. The tracer concentration is measured by an appropriate device at the outlet of the extruder. This leads to concentration curves named  $E(t)$  and  $F(t)$  curves, also known as normalised residence time distribution function and cumulative exit age distribution function, respectively. Both functions can be transformed into each other following Eq. (1) and (2) [18].

$$F(t) = \int_0^t E(t) dt \quad (1)$$

or conversely

$$E(t) = \frac{dF(t)}{dt} \quad (2)$$

The mean residence time  $\bar{\tau}$  and the variance  $\sigma^2$  can be derived from  $E(t)$  according to Eq. (3) and (4).

$$\bar{\tau} = \int_0^{\infty} t \cdot E(t) dt \quad (3)$$

$$\sigma^2 = \int_0^{\infty} (t - \tau)^2 \cdot E(t) dt \quad (4)$$

The standard deviation  $\sigma$  of the RTD curve can be derived by the square root of the variance  $\sigma^2$ .

For characterizing the extruder, the theoretical number of steps  $N$  is of high importance. It can be derived from the mean residence time  $\bar{\tau}$  and the variance  $\sigma^2$  following Eq. (5).

$$N = \left( \frac{\bar{\tau}^2}{\sigma^2} \right) \quad (5)$$

### 3. EXPERIMENTAL SETUP AND VALIDATION DATA

The counter-current extraction process is performed in a screw extractor with a total length  $L$  of 0.320 m. The dried *Artemisia Annuua* leaves are introduced into the extractor at the left side of the horizontal extruder and are conveyed by the screw towards a perforated disc. There, an extraction cake forms due to the increasing pressure induced by the screw rotation. This cake prevents a solvent leakage at the raffinate outlet. Consequently, the introduced solvent flows in counter-current direction to the leaves resulting in high contact times and contact surfaces between both phases. This leads to a high extraction efficiency, resulting in high amounts of the active substance artemisinin in the extract (Figure 1).

To validate the results of the numerical model and consequently its applicability, experiments have been performed. The operating conditions and procedure for reaching a continuous process are summarised here briefly in the interest of space. They will be described in a dedicated publication.

The active substance artemisinin has a low polarity and, hence, a poor solubility in water [19]. Consequently, organic solvents like hexane or toluene should be used for high extraction efficiencies since they provide high solubility values [20,21]. Considering that the performed CFD simulations neglects mass transfer processes between the phases, water has been used as solvent to simplify the experiments.

For measuring the residence time of the solvent, a 10 % concentrated sodium chloride - water solution has been implemented after reaching a quasi-steady state, which took visually 30 minutes. The conductivity of the extract has been measured every minute, repeating three times each experiment.

The extraction cake at the perforated disc does not significantly influence the extraction efficiency of the process; the substance artemisinin has already been almost completely extracted at this location.

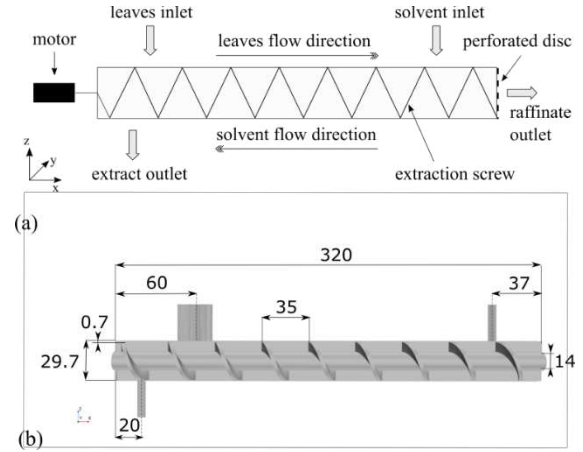


**Figure 1. Counter-current screw extraction process (a) schematically and (b) with important dimensions (in mm) along a vertical cut-plane.**

Nevertheless, the stability of the extraction cake is very important for reaching a quasi-steady state. Consequently, the width of the extraction cake is constant for all possible steady-state operations.

This work focusses on one continuous steady state operating point in the experimentally defined operating window. To capture possible deviations three repetitions of this operating point have been performed. The operating conditions and the averaged residence times of leaves and solvent measured in the experimental setup are listed in Table 1.

**Table 1. Operating conditions and output parameters for the observed steady state.**

Input		Value	Unit
mass flow			
leaves	$\dot{m}_L$	$1.05 \cdot 10^{-3}$	kg/min
solvent	$\dot{m}_S$	$2.08 \cdot 10^{-2}$	kg/min
screw rotation rate			
	$n$	2.2	rpm
Output			
residence time			
perforated disc	$\bar{\tau}_{SL,PD}$	15.45	min
extraction cake	$\bar{\tau}_{SL,EC}$	9.74	min
solvent	$\bar{\tau}_S$	4.87	min
width			
extraction cake	$w_{EC}$	$5 \cdot 10^{-3}$	m
density			
soaked leaves	$\rho_{SL}$	922	kg/m <sup>3</sup>

The averaged residence time of leaves  $\bar{\tau}_{SL,PD}$  describes the final outcome at the perforated disc. Previous measurements at several sampling points inside the extruder showed that the constant axial velocity of leaves in the extruder decreases significantly at the perforated disc due to the compression process. Since the extraction cake does not play a significant role for the extraction efficiency the residence time of leaves in front of the

extraction cake  $\bar{\tau}_{SL,EC}$  is of higher interest and has been used in this work for further estimations.

The dry *Artemisia Annuua* leaves absorb solvent during their transport towards the perforated disc. This absorbed solvent can be called internal extract. To consider this internal extract in the mass flow balance a storage factor  $s$  was measured. This storage factor describes how much mass of solvent is absorbed by 1 g of dry leaves in equilibrium state. For the used solvent (water) this value has been determined as 4.34 by observing several batch mixtures until equilibrium state. The theoretical extract mass flow  $\dot{m}_E$  and raffinate mass flow  $\dot{m}_R$  can be calculated using Eq. (6) and (7).

$$\dot{m}_E = \dot{m}_S - (\dot{m}_L \cdot s) \quad (6)$$

$$\dot{m}_R = (\dot{m}_L + \dot{m}_S) - \dot{m}_E \quad (7)$$

The experimental observations provide important information for setting up the numerical model in order to measure the RTD and the solid-liquid contact areas.

#### 4. NUMERICAL MODEL

The flow investigation was performed with the commercial CFD software package StarCCM+ (Simcenter STAR-CCM+ 2021.3 Build 16.06.008). The dimensions of the computational geometry correspond exactly to the experimental setup (Figure 1). According to a previously performed mesh-independence study a block-structured mesh has been generated with a total number of 1,020,570 finite-volume cells. With this resolution numerical diffusion caused by the mesh can be reduced leading to an accurate representation of the solvent flow behaviour. The screw rotation has been realised by separating the domain into a rotating and a stationary one. Since the rotation is very slow (2.2 rpm) the flow can be assumed as laminar. A Eulerian-based Volume of Fluid (VoF) model has been used to resolve sharply the gas/liquid interface. Initially this free surface is located in the  $x$ - $y$  plane at  $z = 0$  (Figure 2 (a)). To stabilize the free surface and reduce the costs for this multiphase simulation the solvent inlet has been rotated by  $90^\circ$  around the  $x$ -axis, to ensure that liquid solvent directly enters the initially implemented liquid phase. The boundary conditions resulting from the described setup and the simulation mesh are shown in Figure 2.

As the extraction cake does not play an important role for the extraction efficiency it has been neglected in this work. Consequently, the soaked leaves do not enter or exit the process in CFD. They remain at their fixed (steady-state) position and are represented by an additional rotating geometry distributed along the screw and turning with it in a solid movement. Companion experiments showed

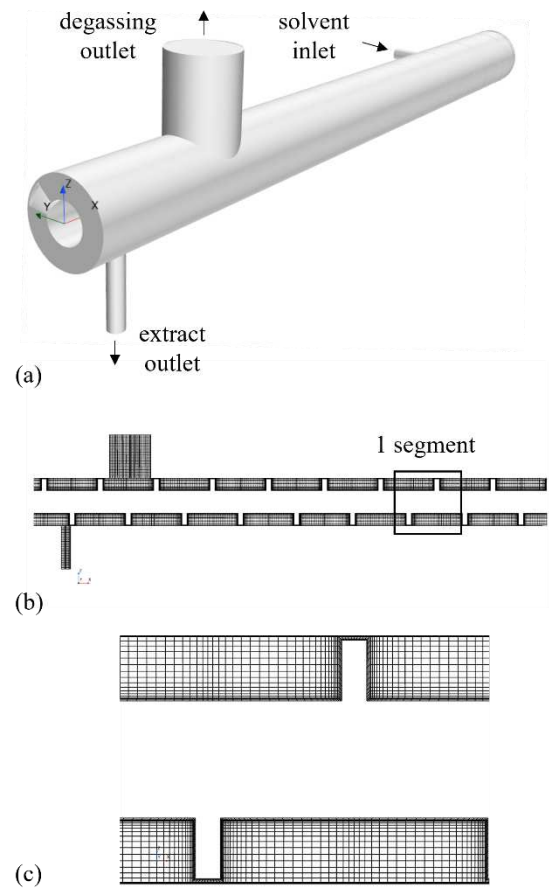


**Figure 2. (a) 3D geometry for CFD simulation with boundary conditions, (b) 3D grid on a vertical plane with a block-structured mesh, (c) detailed grid for one segment showing gaps between screw and wall.**

that the distribution of the soaked leaves during their transport from inlet to raffinate outlet stays nearly constant during the process at steady-state. Visually, the solid phase can be clearly separated from the solvent phase in the transparent extractor. The inlet mass flow rate of solvent has been set to the calculated extract mass flow rate according to Eq. (6), including the loss of solvent during the extraction process due to the absorption by the leaves.

A constant position of the solid-phase distribution in the extruder has been implemented. The total volume of the soaked leaves  $V_{SL,t}$  in the extruder is composed of the distributed volume of soaked leaves in all segments  $V_{SL}$  and the volume of the extraction cake  $V_{EC}$ . It can be calculated according to Eqs. (8) to (10) by using the observed output parameters in Table 1 and the calculated raffinate mass flow according to Eq. (7). The inner and outer screw diameter  $D_i$  and  $D_o$  can be taken from Fig. 1 (b).

$$V_{SL,t} = V_{SL} + V_{EC} \quad (8)$$

$$V_{SL} = \frac{\dot{m}_R \cdot \bar{\tau}_{SL,EC}}{\rho_{SL}} \quad (9)$$

$$V_{EC} = \frac{\pi}{4} \cdot (D_o - D_i)^2 \cdot w_{EC} \quad (10)$$

Since the solid phase is fixed in space and rotates with the screw, a transient measurement of the solid phase RTD in CFD is not possible; consequently, only a rough theoretical assumption is proposed. According to Eq. (9) the residence time depends on the volume of soaked leaves inside the extruder. By setting the experimental and numerical solid volumes equal, the resulting residence times become also comparable since all dimensions, material properties and operating parameters are the same.

For validation procedure the experimental solvent volume has been calculated by using the solvent residence time and the extract mass flow rate (Table 1 and Eq. (6)). The solvent density  $\rho_S$  equals the liquid phase density in Table 2.

$$V_S = \frac{\dot{m}_E \cdot \bar{\tau}_S}{\rho_S} \quad (11)$$

The implementation of an adaptive time step model using a convective mean CFL number ensures the stability of the simulation and an accurate representation of the free liquid surface. Table 2 summarises the used physical models and parameters.

For analysing the residence time distribution of the solvent at the extract outlet, the species method has been used which is involved in StarCCM+ as the passive scalar model. First, the flow has been solved until reaching steady state. This is observed visually after 4 or 5 rotations of the screw. Starting from this time, each rotation delivers similar outflows of solvent and velocities. To investigate this point in more detail, both quasi-steady state conditions (obtained after 4, or 5 rotations of the screw) have been considered in the analysis. The flow field at quasi-steady state is then frozen and the tracer species has been initialised, tracking only convection processes. A constant time step of 0.1 s has been implemented for this post-processing step, allowing short calculation times. Finally, an additional transport equation is solved in the domain for the tracer species.

**Table 2. Physical models and parameters.**

Description	Settings
Discretization scheme: momentum	2nd order
Under-relaxation factor	
Velocity	0.4
Pressure	0.2
Discretization scheme: volume fraction	2nd order
Under-relaxation factor	
Volume fraction	0.2
Temporal discretization	1st order
Adaptive time step criteria	
Convective mean CFL number	1
Minimum time step (s)	1E-4
Maximum time step (s)	0.01
Inner iterations	10
Boundary conditions	
Solvent inlet	Mass flow inlet
Extract outlet	Split outlet
Degassing outlet	Pressure outlet
Operating pressure (Pa)	101325.0
Mass flow solvent (kg/s)	$2.71 \cdot 10^{-4}$
Gravity in vertical direction (z)	-9.81
Liquid phase (water)	
Density (kg/m <sup>3</sup> )	997.56
Viscosity (Pa·s)	$8.89 \cdot 10^{-4}$
Gas phase (air)	
Density (kg/m <sup>3</sup> )	1.18
Viscosity (Pa·s)	$1.86 \cdot 10^{-5}$

## 5. RESULTS

### 5.1. Validation of phase distribution

The solvent residence time depends on its volumetric flow rate and on the free volume in the extruder, which is influenced by the fixed solid phase volume in the model employed here. To ensure the compatibility of this assumption one segment has been observed and compared with experiments.

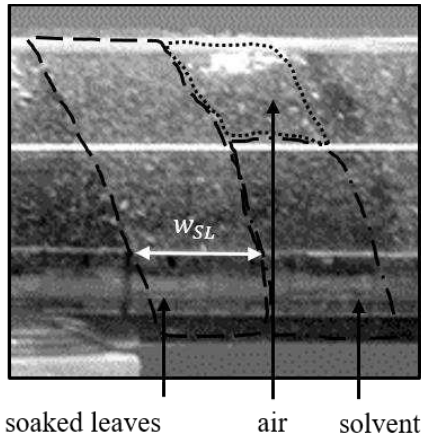
The volume of the soaked leaves and the solvent in the numerical model have been calculated theoretically according to Eq. (8) and (11) by using the experimentally measured residence time, respectively.

Table 3 shows a good agreement of the resulting width of soaked leaves in one segment estimated from the experimental image in

Figure 3 (CFD:  $1.67 \cdot 10^{-2}$  m, Exp: 1.6 -  $1.7 \cdot 10^{-2}$  m).

**Table 3. Results from the soaked leaves volume for experiments and CFD.**

Parameter	Exp	CFD	error (%)
total volume ( $10^{-5} \text{ m}^3$ )	$V_{SL,t}$ 6.02	6.13	1.8
width in segment ( $10^{-2} \text{ m}$ )	$w_{SL}$ 1.6 - 1.7	1.67	-



**Figure 3. Experimental phase distribution in one segment.**

Experimental observations of the water surface can only be estimated roughly. It is hindered by soaked leaves sticking to the inner wall of the extractor. Figure 4 shows a comparison of the calculated total solvent volume in experiments with  $\pm 5\%$  range and the determined CFD solvent volume after each screw turn. After reaching the quasi-steady state at four screw turns the solvent volume fits into the experimental volume range. Further screw turns show similar values ensuring the quasi-steady state.

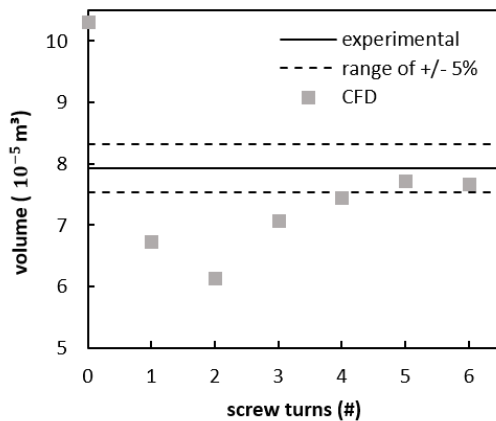


**Figure 4: Comparison of total solvent volume between experiments with  $\pm 5\%$  range and CFD data after each screw turn.**

Consequently, the phase distribution appears to be represented sufficiently well by the numerical simulation.

## 5.2. Residence Time Distribution of solvent phase

The residence time distribution (RTD) of the solvent phase in CFD has been measured by using the species method for two quasi-steady state conditions (after 4 or 5 full rotations of the screw). The resulting RTD curves are shown in Figure 5 and compared with the experimentally measured RTD curves, involving three identical runs. Although all three repetitions have identical operating conditions, minor deviations are found in the results. These can occur due to minute changes in local particle distributions, particle-particle interactions, or small variations in the screw rotation speed.

Comparing the numerical RTD curves with the experimental RTD data, a good agreement can be observed. Nevertheless, there are still deviations between numerical and experimental results. Both numerical curves increase faster and show a higher maximum than the experimental curve (Exp: 0.22 1/min, CFD: 0.275 1/min).

Analysing the mean residence time and its standard deviation for both steady-state conditions, the obtained agreement is still found to be quite good (Table 4). The experimental mean residence time of 4.87 min is higher than both numerically calculated residence times (4 turns: 4.08 min, 5 turns: 3.70 min). However, considering additionally the standard deviation, the numerical results fit into the experimentally measured range. The deviations between the numerical residence times ( $\pm 10\%$ ) result from the performed quasi-steady state with unsteady solver. Consequently, the liquid velocity profile differs slightly for each screw rotation influencing the species movement.

Furthermore, the calculated theoretical number of steps  $N$  results in a value of three for both experiments and CFD. This indicates a good representation of the RTD behaviour by our CFD model.

**Table 4. Results of numerical RTD study and comparison to deviations observed when repeating the experiments.**

Operation	$\bar{\tau}$ (min)	$\sigma$ (min)	$N$ (-)
Exp	4.87	$\pm 2.96$	3
CFD			
4 turns	4.08	$\pm 2.28$	3
5 turns	3.70	$\pm 2.03$	3

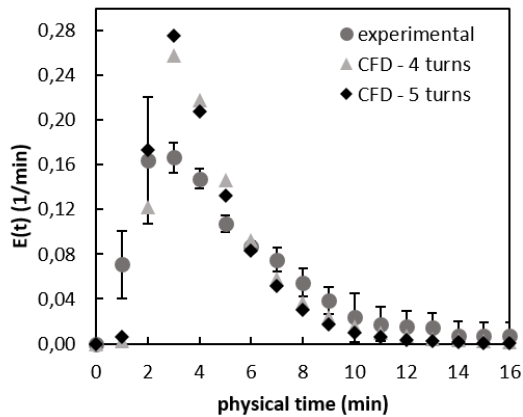


**Figure 5: Results from the solvent RTD study by comparing the deviations observed when repeating three experimental runs with two quasi-steady states of the CFD simulation (after 4 and 5 screw turns).**

### 5.3. Contact area

The contact area between the solid leaves and the liquid solvent influences the reaction kinetics since mass transfer processes take place at this location. In the described model the leaves are not represented as single particles and consequently the exact mass transfer areas cannot be determined. Nevertheless, it has already been shown that the CFD simulation can capture the phase distribution in the extruder. This allows an approximation of the contact surfaces by using the Eulerian particle phase. Figure 6 represents the determined contact areas in the screw extruder starting from the extract outlet (segment one) for 4 and 5 turns of screw rotation (the two quasi-steady states considered previously).

The contact areas for both observations are very similar, showing again that quasi-steady state has been reached. At the extract outlet no leaves are present, which results in a zero-contact area. With increasing length of the extruder, the contact area increases and stabilizes at a value of approx.  $3.5 \cdot 10^{-4} \text{ m}^2$  in the middle segments 3 - 7. The largest contact area appears in the segment 9 that is located between the inlet of solvent and the extraction cake. At this position fresh solvent is introduced in the extractor and is pushed by the screw towards the extraction cake. Consequently, higher water surfaces arise and contact areas between leaves and solvent increase.

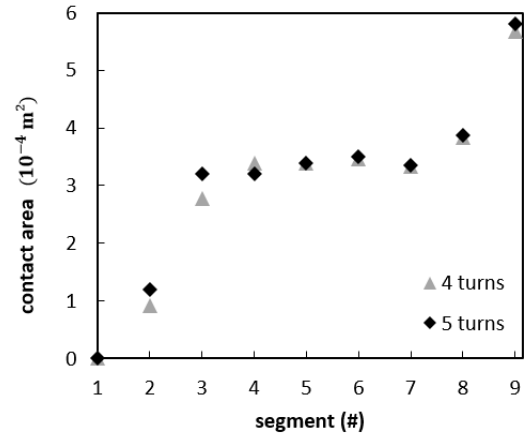


**Figure 6. Contact area between leaves and solvent for two quasi-steady states in CFD for all segments starting from the extract outlet (segment 1).**

## 6. CONCLUSIONS

In this study the residence time distribution of a liquid solvent has been analysed in a counter-current screw extractor by using 3D CFD simulations. According to companion experiments the soaked leaves phase is equally distributed between inlet and outlet. Consequently, the theoretically estimated leaves volume was implemented as a constant rotating geometry. This allowed short calculation times due to a reduced model, a two-phase flow of liquid and gas phase that has been solved with the Volume of Fluid (VoF) approach. Since the solvent residence time depends on the free volume in the extractor an optical validation of the model assumptions has been first performed in one screw segment, showing a good agreement. The comparisons of the RTD confirm the good estimation of the residence time by using the described model. The two selected quasi-steady states deliver residence times of 4.08 min (4 screw turns) and 3.70 min (5 screw turns), fitting into the range of the experimental measurements when considering repeatability. The CFD number of steps is equal to that of the experiments, demonstrating a good representation of the counter-current process. The resulting contact areas of leaves and solvent in the segments are an important information for mass transfer interactions during the actual extraction process.

In future studies these contact areas shall help to parametrize compartment models (CM), in order to consider mass transfer interactions with acceptable computational times. This combined CFD/CM model shall ultimately be used to optimise the extraction process and increase the extraction efficiency of artemisinin from *Artemisia Annua* leaves.

## ACKNOWLEDGEMENT

The authors gratefully acknowledge the support given by the International Max Planck Research School for Advanced Methods in Process and Systems Engineering (IMPRS ProEng).

## REFERENCES

- [1] Bart, H.-J., Pilz, S., 2011, *Industrial Scale Natural Products Extraction*, Wiley-VCH, Weinheim.
- [2] World malaria report 2021, Geneva: World Health Organization, 2021, Licence: CC BY-NC-SA 3.0 IGO.
- [3] Gilmore, K., Kopetzki, D., Lee, J.W., Horváth, Z., McQuade, D.T., Seidel-Morgenstern, A., Seeberger, P.H., 2014, "Continuous synthesis of artemisinin-derived medicines", *Chemical communications*, Vol. 50, pp. 12652–12655.
- [4] Eitzlmayr, A., Matić, J., Khinast, J., 2017, "Analysis of flow and mixing in screw elements of corotating twin-screw extruders via SPH", *AIChE J*, Vol. 63, pp. 2451–2463.
- [5] Kovacevic, A., Rane, S., Stosic, N., 2016, "Computational fluid dynamics in rotary positive displacement screw machines", *16th International Symposium in Transport Phenomena and Dynamics of Rotating Machinery*, HAL archives-ouvertes.fr.
- [6] Ferreira, M.C., Gonçalves, D., Bessa, L.C., Rodrigues, C.E., Meirelles, A.J., Batista, E.A., 2022, "Soybean oil extraction with ethanol from multiple-batch assays to reproduce a continuous, countercurrent, and multistage equipment", *Chemical Engineering and Processing - Process Intensification*, Vol. 170, 108659.
- [7] Dhekne, P.P., Patwardhan, A.W., 2021, "CFD model for transient flow fields around teabag during tea infusion", *Food and Bioprocess Proceedings*, Vol. 130, pp. 79–91.
- [8] Turgut, S.S., Feyissa, A.H., Baltacioglu, C., Kucukoner, E., Karacabey, E., 2020, "Extraction simulation of porous media by CFD: Recovery of trans-resveratrol from grape cane by pressurized low polarity water system", *Chemical Engineering and Processing - Process Intensification*, Vol. 148, 107779
- [9] He, A., Zhang, N., 2012, "CFD for cyclone optimization for liquid extraction from solid particles in turbulent air flows", *ASME International Mechanical Engineering Congress and Exposition, Proceedings (IMECE)*, Vol. 7, pp. 183–187.
- [10] Shokrian, A., Mobli, H., Akbarnia, A., Jafari, A., Mousazade, H., Zhu, B., 2019, "A study on the three-phase separator machine (tricanter) for olive oil extraction", *Journal of Theoretical and Applied Mechanics*, Vol. 49, pp. 233–240.
- [11] Wang, Y., Herdegen, V., Repke, J.-U., 2016, "Numerical study of different particle size distribution for modeling of solid-liquid extraction in randomly packed beds", *Separation and Purification Technology*, Vol. 171, pp. 131–143.
- [12] Dadashi, A., Zhu, J., Zhang, C., 2014, "CFD modelling of continuous protein extraction process using liquid-solid circulating fluidized beds", *The Canadian Journal of Chemical Engineering*, Vol. 92, pp. 1911–1919.
- [13] Bednarz, A., Weber, B., Jupke, A., 2017, "Development of a CFD model for the simulation of a novel multiphase counter-current loop reactor", *Chemical Engineering Science*, Vol. 161, pp. 350–359.
- [14] Gillani, S.S.J., Ullah, A., Zaman, M., Chughtai, I.R., Inayat, M.H., 2017, "Counter-current three-phase fluidization in a turbulent contact absorber: A CFD simulation", *Particuology*, Vol. 35, pp. 51–67.
- [15] Chen, K., Bachmann, P., Bück, A., Jacob, M., Tsotsas, E., 2019, "CFD simulation of particle residence time distribution in industrial scale horizontal fluidized bed", *Powder Technology*, Vol. 345, pp. 129–139.
- [16] Tan, H., Wen, N., Ding, Z., 2021, "Computational fluid dynamics simulation of multi-phase flow characteristics in an industrial-scale randomly packed tower", *Asia-Pac J Chem Eng*, Vol. 16, e2708.
- [17] Yang, L., Liu, F., Song, Z., Liu, K., Saito, K., 2018, "3D Numerical Study of Multiphase Counter-Current Flow within a Packed Bed for Post Combustion Carbon Dioxide Capture", *Energies*, Vol. 11, 1441.
- [18] Levenspiel, O., 1999, *Chemical Reaction Engineering. 3rd edition*, John Wiley & Sons.
- [19] Haynes, R.K., Fugmann, B., Stetter, J., Rieckmann, K., Heilmann, H.D., Chan, H.W., Cheung, M.K., Lam, W.L., Wong, H.N., Croft, S.L., Vivas, L., Rattray, L., Stewart, L., Peters,

W., Robinson, B.L., Edstein, M.D., Kotecka, B., Kyle, D.E., Beckermann, B., Gerisch, M., Radtke, M., Schmuck, G., Steinke, W., Wollborn, U., Schmeer, K., Römer, A., 2006, "Artemisone - A highly active antimalarial drug of the artemisinin class", *Angewandte Chemie International Edition*, Vol. 45, pp. 2082-2088.

[20] Lapkin, A.A., Plucinski, P.K., Cutler, M., 2006, "Comparative assessment of technologies for extraction of artemisinin", *Journal of natural products*, Vol. 69, pp. 1653–1664.

[21] Liu, Y., Lü, H., Pang, F., 2009, "Solubility of Artemisinin in Seven Different Pure Solvents from (283.15 to 323.15) K", *Journal of Chemical & Engineering Data*, Vol. 54, pp. 762–764.